# *Behavior of eccentrically loaded double circular steel tubular short columns filled with concrete*

Ahmed, M., Liang, Q. Q., Patel, V. I. and Hadi, M. N. S. (2019). Behavior of eccentrically loaded double circular steel tubular short columns filled with concrete. *Engineering Structures*, 201: 109790.

# Behavior of eccentrically loaded double circular steel tubular short columns filled with concrete

Mizan Ahmed[a], Qing Quan Liang[a,1], Vipulkumar Ishvarbhai Patel[b], Muhammad N. S. Hadi[c]

[a] *College of Engineering and Science, Victoria University, PO Box 14428, Melbourne, VIC 8001, Australia*
[b] *School of Engineering and Mathematical Sciences, La Trobe University, Bendigo, VIC 3552, Australia*
[c] *School of Civil, Mining and Environmental Engineering, University of Wollongong, Wollongong, NSW 2522, Australia*

## ABSTRACT

Circular concrete-filled double steel tubular (CFDST) columns in high-rise building structures possess high ductility and strength performance owing to the concrete confinement exerted by the external and internal circular steel tubes. However, the behavior of circular CFDST short columns that are loaded eccentrically has not been investigated either experimentally or numerically. Particularly, numerical studies on the moment-curvature responses, strength envelopes, confinement effects and moment distributions in circular CFDST beam-columns have not been reported. In this paper, experimental and computational investigations into the structural responses of circular CFDST short columns loaded eccentrically are presented. Nineteen short circular CFDST columns with various parameters under axial and eccentric loads were tested to failure to measure their structural responses. Test results are presented and discussed. A mathematical simulation model underlying the method of fiber analysis is proposed that simulates the axial load-moment-curvature relationships as well as the strength interaction curves of CFDST beam-columns composed of circular sections. The mathematical modeling technique explicitly takes into account the confinement of concrete on the responses

[1]Corresponding author.
*E-mail address:* Qing.Liang@vu.edu.au (Q. Q. Liang)

of CFDST columns. The computational procedure and solution method are given. The accuracy of the computer simulation model is evaluated by comparing computations against experimental data. The significance of material and geometric properties, concrete confinement and axial load ratio on the responses of moment-curvature and strength envelopes of CFDST columns and the moment distributions in concrete and steel components are investigated. The mathematical model proposed not only simulates well the experimentally observed responses of CFDST columns but also can monitor the moment distributions in the steel and concrete components of such composite columns.

*Keywords: Concrete-filled double steel tubes; beam-columns; composite columns; fiber element modeling; nonlinear analysis; short columns.*

## 1. Introduction

Circular concrete-filled double steel tubular (CFDST) columns as schematically depicted in Fig. 1 have increasingly been used in high-rise as well as super high-rise buildings to support heavy loads because of their high ductility and strength performance. The circular CFDST column may be formed by strengthening an existing concrete-filled steel tubular (CFST) circular column with an outer circular steel tube that is filled by either normal or high strength concrete. In a circular CFDST column loaded in compression, the inner steel tube effectively confines the core-concrete while the external tube exerts confinement to both the sandwiched-concrete and the core concrete [1-3]. The effective design of a CFDST column may be achieved by using the outer and inner tubes with different strengths and filling the tubes with concrete of different strengths. In composite buildings, CFDST columns are often subjected to eccentric loads. Therefore, understanding their performance under eccentric loading is vital for effective

design purpose. The current design codes, which include Eurocode 4 [4] and ANSI/AISC 360-16 [5], have not provided design rules for designing circular CFDST beam-columns because experimental and computational studies on their behavior have been extremely rare. This paper addresses this issue.

The experimental behavior of CFDST short columns composed of circular steel sections that were loaded axially has been reported by a number of investigators [6-9]. Test results presented by Xiong et al. [6] showed that utilizing an internal circular tube increased the ultimate axial loads of short circular CFDST columns significantly. However, the effect of the internal tube was more pronounced on the CFDST columns constructed by normal strength concrete than those made of ultra-high-strength concrete. They also studied the effects of using concrete with different strengths to fill the sandwiched space and the internal tube on the structural behavior of CFDST columns. Peng et al. [7] reported that the ultimate loads of the tested circular CFDST columns decreased with increasing the diameter-to-thickness ratio of the steel tubes. The CFDST slender and short columns loaded in axial compression by Wan and Zha [8] failed in a ductile manner. It was reported that increasing the steel ratio of the internal tube improved the ultimate strengths of CFDST short and slender columns markedly. Ekmekyapar and Al-Eliwi [9] investigated the possibility of repairing highly deformed CFST column by placing an outer tube and filling the hollow section with concrete to form a CFDST column. It was observed that the repaired CFST columns exhibited similar performance to that of the freshly fabricated CFDST columns. However, the tested CFDST columns failed prematurely due to the lack of sufficient end restraints. Moreover, Romero et al. [10] performed tests on circular CFDST slender columns at ambient and elevated temperatures. The parameters chosen for the study included the thickness of steel tubes as well as concrete strength. Ibañez et al. [11] investigated the influences of ultra-high-strength concrete on the structural behavior of CFDST slender

circular columns that were under eccentric compression. Chang et al. [2] and Zheng et al. [12] studied the strengths of concrete-filled stainless steel-carbon steel tubular (CFSCST) columns with an external stainless steel tube. However, as discussed by Patel et al. [13, 14] owing to the difference of the material behaviors between carbon steel and stainless steel, the performance of CFSCST columns is different from that of CFDST columns.

Computer modeling techniques have been employed to compute the performance of nonlinear inelastic circular CFDST columns that were loaded concentrically [1, 3, 8, 15, 16]. Chang et al. [2] and Hassanein et al. [3] developed finite element (FE) models for analyzing nonlinear short CFSST columns using the general-purpose FE program ABAQUS. The lateral pressure on the core-concrete was computed by simply adding the lateral pressures induced by the outer stainless-steel tube and by the inner carbon-steel tube. Zheng and Tao [15] developed FE models for circular and square CFDST columns and suggested design equations to estimate the ultimate strength, compressive stiffness and ultimate strain of CFDST columns. The material laws of steel proposed by Katwal et al. [17] and the stress-strain curve for concrete given by Tao et al. [18] were utilized to model the behavior of CFDST columns. The confinement exerted by the external tube on the strength enhancement of the core-concrete was not considered, but confinement factors for the sandwiched-concrete and core-concrete were used. It was shown that the FE models predicted well the structural behavior. Ahmed et al. [1] developed a new confinement model based on the available experimental data for the core-concrete in circular CFDST columns while the lateral pressures provided by the external steel tube to the sandwiched-concrete were quantified using the model of Hu et al. [19]. The computational technique implementing the new confinement model predicted well the behavior of CFDST short circular columns that were axially loaded.

It would appear that no experimental and computational studies on the responses of short CFDST columns composed of circular sections under eccentric loading have been reported. In this paper, experimental and computational investigations into the structural performance of short CFDST circular columns loaded eccentrically are presented for the first time. The paper is organized as follows. The test program is presented first and the test results obtained are then described. The nonlinear numerical analysis procedure for modeling the moment-curvature behavior and strength envelopes of CFDST columns is presented. This is followed by the experimental verification of the numerical procedure. Parametric studies on the structural performance of CFDST short columns that are eccentrically loaded are conducted by means of utilizing the computer model developed and the results obtained are discussed.

## 2. Test program

### *2.1. General*

A total of nineteen short CFDST columns composed of circular tubes were tested to failure to investigate their structural performance. The short columns were loaded either axially or eccentrically during the tests. This is for the very first time, tests on eccentrically loaded circular short CFDST columns had been carried out. The test parameters mainly focused on the application of loading (axial and eccentric), the diameter-to-thickness ratios of the inner and outer steel tubes and loading eccentricity.

### *2.2. CFDST column specimens*

The hollow circular tubes of CFDST column specimens were constructed by cold-formed thin-

walled steel tubes, which were cut into the design length from the long steel tubes supplied by the steel supplier. The specimen length was three times the diameter of the external tube to prevent the column from overall buckling. A typical circular CFDST short column specimen is depicted in Fig. 1, where $D_o$ and $t_o$ are the outer diameter and thickness of the external tube; $D_i$ and $t_i$ the outer diameter and thickness of the internal tube. The column specimens were divided into four groups namely Groups G1, G2, G3 and G4. The material properties as well as geometry of column specimens are given in Table 1, where $f_c^{'}$ is the compressive strength of concrete cylinder, $e$ the loading eccentricity, and $P_{u,\exp}$ the experimental ultimate load. Each group consisted of 5 column specimens in which two identical specimens were loaded concentrically to failure except Group G1. The nominal cross-sectional dimensions of the outer steel tubes in Groups G1 and G3 were 139.7× 5.0 mm while those in Group G2 and G4 were 165.1× 5.0 mm. The nominal sizes of the inner tubes in Group G1, G2, G3 and G4 were 76.1×3.6 mm, 88.9×4.0 mm, 76.1×3.2 mm and 88.9×3.2 mm, respectively. The fabrication of CFDST column specimens was performed by placing the outer and inner hollow steel tubes concentrically and the two tubes were welded with two steel bars to secure their concentric position. Six stiffeners of 32×50 mm with the same thickness as the tube were welded to the ends of the circular outer steel tube around the circumference at $60°$ apart to avoid premature local buckling at the column end during the test. Ready-mix concrete was utilized to fill the hollow steel tubes. Two different concrete mixes were employed where the aggregate size was 12 mm. The concrete was poured into the tubes in layers and compacted by using a vibrator.

### *2.3. Material properties*

Tensile coupon samples were cut from the steel tubes that were employed to fabricate the circular CFDST columns. Two coupon samples were prepared from each tube and tested

according to the requirements of AS 1391 [20]. The curves of stress and strain for the tensile coupon samples are presented in Fig. 2, where the cross-sectional dimensions of the tube were used to identify the individual curve associated with a code designated by C1 or C2. The steel yield strengths of coupon samples varied from 332 to 412 MPa while their tensile strengths ranged from 372 to 510 MPa. The strains of the test coupon samples corresponding to the tensile strength ranged from 0.17 to 0.27 with an average value of 0.21. The measured yield strengths, tensile strengths and their corresponding strains with the calculated modulus of elasticity are listed in Table 2.

Concrete cylinders (100 mm × 200 mm) were also casted and cured in the same environment as the circular CFDST column specimens. Compression tests on concrete cylinders were undertaken to determine their compressive concrete strengths at least after 28 days of the casting. The concrete compressive strengths were averaged from 42-cylinder test results collected from the start and end of the experimental work. The average concrete compressive strength for CFDST column specimens in Groups G1 and G2 was 19.1 MPa while for Groups G3 and G4 it was 20.6 MPa. The reason for using the low strength concrete was because all column specimens were originally designed to be tested using the 2000 kN compression testing machine at Victoria University, Australia. However, due to the failure of the machine, all column specimens were then tested at the University of Wollongong, Australia.

### *2.4. Test set up*

All circular CFDST column specimens were loaded to failure using the Denison compression testing machine having 5000 kN capacity at the structure laboratory in the School of Civil, Mining and Environmental Engineering at the University of Wollongong, Australia. The actual

test configurations of column specimens under axial loading and eccentric loading are illustrated in Fig. 3. As shown in Fig. 3(a), for column specimens subjected to concentric loading, the compression load was directly applied on the column specimens. The ends of axially loaded CFDST column specimens were grinded using a concrete grinder to ensure maximum uniform contact between the specimens and the loading heads of the machine. On the other hand, the specially designed loading heads were utilized to simulate the pined-end conditions of the column specimen that was eccentrically loaded as illustrated in Fig. 3(b). The loading heads, which were designed by Hadi and Widiarsa [21], had a round adaptor plate and a 25 mm thick bottom steel plate with a ball joint. The loading heads were grooved with different offsets to obtain different loading eccentricities. Both ends of the column specimen were plastered to the loading heads. The strain distributions of circular CFDST columns were measured by strain gauges. Two strain gauges were mounted at the mid-height of the column specimen under axial compression where one strain gauge was used to capture the axial strain and another strain gauge was used to record the transverse strain of the columns. However, for the column specimen subjected to eccentric loading, both strain gauges were mounted at the compression and tension sides of the column mid-height to record the axial strain only. Two linear variable differential transducers (LVDTs) were installed at the opposite corners of the testing machine to measure the axial shortening of the column specimen as illustrated in Fig. 3. An additional laser triangulation was employed to measure the deflection at the mid-height of the column specimen tested under eccentric loading as shown in Fig. 3(b).

The column specimen was initially preloaded to 100 kN at a rate of 1.67 kN/s to prevent any slip that could occur during the tests and then unloaded to 20 kN before finally started recording the data. The column specimens were loaded by using the displacement control method with a

rate of 0.8 mm/min until failure. A digital data acquisition system was employed to record the readings of LVDTs, strain gauges, laser triangulation and applied load.

## 3. Test results and discussions

### *3.1. CFDST column specimens under axial loading*

Circular CFDST short column specimens were tested up to large axial deformations. The stopping criterion for testing was either the column specimen buckled significantly or the axial load increment became small enough around the axial shortening of 30 mm. The failure of the column specimens loaded concentrically was caused by the outward local buckling of the outer steel tube as shown in Fig. 4 and the concrete crushing at the locations of the tube local buckling. Figure 4 demonstrates that the stiffeners successfully prevented the local failure of the column ends from occurring. It can be observed from the sectional view of Specimen CC10 presented in Fig. 5 that there was a composite interaction between the external tube and the sandwiched-concrete and that between the internal tube and core-concrete. The crushing of the sandwiched concrete took place at the regions where the steel tube buckled locally. However, the local buckling of the internal steel tube was effectively prevented by the rigid concrete.

The measured axial load-axial shortening curves of CFDST columns have been plotted in Fig. 6 and ultimate axial loads ($P_{u,\exp}$) are tabulated in Table 1. It would appear from Fig. 6 that CFDST circular columns have a good ductility as well as large deformation capability. The axial load-shortening curves of the two columns loaded axially in each group are almost the same. Due to the concrete confinement, the ultimate loads of axially loaded columns in Groups G1, G2, G3 and G4 are 23.6%, 11.6%, 26.4% and 31.9% higher than their theoretical ultimate

loads without considering concrete confinement. The inconsistency of the increase in the percentage of the ultimate loads of column specimens in Group G2 compared to other Groups was caused by the uncertainty of the actual strengths of concrete in these column specimens as the average concrete compressive strength was employed to calculate the theoretical ultimate loads. It is observed from Table 1 that the column ultimate load increases with an increase in the steel ratio. The $D_o / t_o$ ratios of the column Specimens CC1 and CC10 with the same $D_o$ were 27.9 and 39.9, respectively. The ultimate axial load of Specimen CC1 is 7.6% higher than that of Specimen CC10. Moreover, increasing the $D_o / t_o$ ratio by using a larger diameter of the outer tube increased the cross-sectional areas of the confined concrete and steel. Therefore, the strength of the columns was improved. However, the column ultimate strength was also influenced by the thickness of the external steel tube. The ultimate load of the Specimen CC5 is 7.2% higher than that of Specimen CC1. However, the ultimate axial load of Specimen CC15 is 28.2% higher than that of Specimen CC10. The test results show that the larger the concrete cross-sectional area, the higher the column ultimate load. The reason for this is that the concrete carries most of the load in a CFDST column.

The axial load-axial strain curves in addition to the axial load-hoop strain responses provide important information about the delamination of CFDST columns and contact stresses between the confined concrete and steel tubes. Figure 7 presents the measured axial loads vs axial and hoop strain curves of column specimens that were concentrically loaded. The axial and hoop strains of circular CFDST short columns increased linearly at the elastic stage without confinement because the steel material had a larger Poisson's ratio than the concrete. However, as the load increased, the sandwiched concrete expanded more than that of the outer tube. Therefore, the hoop strains of the column specimens increased rapidly as shown in Fig. 7. The

presence of the hoop strain-induced lateral pressures on the concrete, which increased the compressive strength of the concrete.

### *3.2. CFDST columns under eccentric loading*

The failure of eccentrically loaded CFDST column specimens was caused by the outward local buckling of the outer steel tubes in the compression regions near the mid-height of the column specimens, the concrete crushing at the locations of tube buckling, and the column bending as shown in Fig. 8. For columns under a large loading eccentricity, the external steel tube near the column ends underwent significant buckling. The sandwiched concrete in some column specimens was separated from the inner tubes as depicted in Fig. 9. The section view of Specimen CC13 is illustrated in Fig. 10. It is confirmed that the core-concrete in the CFDST columns loaded eccentrically was confined effectively by the steel tubes and did not crush. The main difference between the fundamental behaviors of circular CFST columns and CFDST columns is that the CFDST column has higher strength and ductility than the CFST column for the same outer tube diameter, steel cross-sectional area and material strengths as reported by Ahmed et al. [1]. Circular CFST short columns under eccentric loading may fail by the outward local buckling and crushing of the concrete in the compression zone. Circular CFDST columns under eccentric loading may fail by the outward local buckling and crushing of the sandwiched concrete in the compression zone, but the core concrete does not crush due to the confinement provided by both steel tubes.

The experimentally measured axial load-shortening curves for the tested specimens have been plotted in Fig. 11. It is clearly illustrated that increasing the loading eccentricity ratio ($e / D_o$) significantly reduces the ultimate axial loads of the column specimens. The ultimate axial loads

of column specimens in Group G4 were reduced by 30%, 43% and 59% by changing the $e / D_o$ ratio from 0 to 0.06, 0.12 and 0.21, respectively. The measured responses of load-axial shortening and axial load-lateral deflection of column specimens under eccentric compression are given in Figs. 11 and 12, respectively, where $u_m$ is the lateral deflection at the column mid-height. It is observed that increasing the $e / D_o$ ratio considerably reduces the axial stiffness of the beam-columns. However, all tested column specimens exhibited good ductility and deformation capability. The measured load vs longitudinal strain distributions for specimens loaded eccentrically are illustrated in Fig. 13. The negative strain represents tensile strain while the positive strain means compressive strain. The measured compressive strains were larger than the tensile strains as can be seen from Fig. 13.

## 4. Nonlinear analysis

### *4.1. Basic concepts*

A mathematical model underlying the theory of fiber analysis is developed to simulate the nonlinear inelastic moment-curvature relationships and strength envelopes of eccentrically loaded circular CFDST columns. The fiber element method is an accurate and computationally efficient numerical modeling method for the simulation of nonlinear composite columns over the traditional finite element method as pointed out by Liang [22] and Ahmed et al. [23]. The typical fiber discretization of the concrete and steel components in the cross-section of a circular CFDST is illustrated in Fig. 14, where $d_n$ is the depth of the plastic neutral axis in the cross-section, $y_i$ the distance from the section centroid to the centroid of the *i*th fiber element, $d_{e,i}$ the distance from the neutral axis to the element centroid, $\phi$ the curvature, $\varepsilon_t$ the compressive

strain at the extreme fiber, and $\varepsilon_{e,i}$ the strain of the *i*th fiber element. The plane section is assumed to remain plane after deformation in the fiber analysis technique. This implies a linear distribution of strains through the depth of the column cross-section as illustrated in Fig. 14. Under the axial loading combined with uniaxial bending, the fiber strain is computed from the curvature and the neutral axis depth of the cross-section [14, 24, 25]. The stresses in steel and concrete fibers are determined from the material uniaxial stress-strain relationships of steel and concrete given in Section 5. The internal force (*P*) as well as moment (*M*) are calculated as stress resultants over the entire cross-section.

*4.2. Computer simulation procedure*

The moment vs curvature curves of circular CFDST columns loaded eccentrically are simulated by increasing the curvature incrementally and computing the corresponding moment. The force equilibrium condition must be maintained for each increment of the curvature by adjusting the neutral axis depth ($d_n$) of the cross-section. The internal moment (*M*) is determined by the integration of fiber stresses over the entire cross-section. The complete moment-curvature curve for a given axial load can be obtained by repeating the process of analysis.

The strength envelope, which represents the axial load ($P_u$) and ultimate moment ($M_u$) interaction diagram, of a short circular CFDST column is used in designing columns subjected to eccentric loading. In the simulation of the interaction curve, the ultimate axial load ($P_o$) of the CFDST column loaded concentrically is firstly calculated by the axial load-strain analysis procedure considering the concrete confinement. The axial load ($P_u$) is increased gradually from zero to the maximum ultimate load ($P_o$), and the corresponding ultimate moment ($M_u$) of

the composite section is ascertained from the moment-curvature relationships. The equilibrium condition for each curvature increment must be maintained by ensuring the internal axial load ($P$) calculated is the same as the applied axial load ($P_u$). To achieve this condition, the neutral axis depth ($d_n$) of the column section is adjusted iteratively by efficient numerical algorithms. The inverse quadratic method has been implemented in the mathematical programming scheme to solve the highly dynamic equilibrium functions [26]. The computer flowchart for calculating the strength envelope of a short CFDST column is given in Fig. 15, where $\Delta\varepsilon$ is the axial strain increment, $P_{\max}$ the maximum axial load that can be applied to the column, $\varepsilon_{cu}$ the ultimate strain of concrete in compression, $\Delta\phi$ the curvature increment, $r_p$ the residual force expressed as $r_p = P_u - P$, and $\Delta P_u$ the axial load increment.

### *4.3. Computational solution algorithms*

Computational solution algorithms implementing the inverse quadratic method have been developed by Ahmed et al. [26, 27] for quantifying the neutral axis depth ($d_n$) during the loading history of CFDST columns. The inverse quadratic method requires three initial values of $d_n$ taken as $d_{n,1} = D_0$, $d_{n,2} = D_0/2$ and $d_{n,3} = \left(d_{n,1} + d_{n,2}\right)/2$ to be initialized to start the computation process. The new true $d_n$ is then calculated by the following equations:

$$d_{n,j+3} = d_{n,j+1} - r_{p,j+1}\left(\frac{A}{C}\right) \tag{1}$$

$$A = (r_{p,j})^2(d_{n,j+2} - d_{n,j+1}) + r_{p,j}r_{p,j+1}(d_{n,j+1} - d_{n,j+2}) + (r_{p,j+1} - r_{p,j+2})r_{p,j+2}(d_{n,j} - d_{n,j+1}) \tag{2}$$

$$C = (r_{p,j+1} - r_{p,j})(r_{p,j+2} - r_{p,j})(r_{p,j+2} - r_{p,j+1}) \tag{3}$$

where the residual force $r_p = P_u - P$ and $j$ is the iteration number. The stopping criterion of the computational process is determined as $\left|r_p\right| < \varepsilon_k$, in which $\varepsilon_k$ is taken as $10^{-4}$.

### *4.4. Curvature ductility index*

The curvature ductility indicator evaluates the ductility of a circular CFDST column eccentrically loaded and is defined as

$$PI_{cd} = \frac{\phi_u}{\phi_y} \tag{4}$$

in which $\phi_u$ denotes the ultimate curvature of the column when the moment falls to 90% of its ultimate moment capacity in the post-peak range or the ultimate curvature where column shows ascending moment-curvature relationships in the post-yield regime. The yield curvature $\phi_y$ is taken as the curvature corresponding to 75% of the column ultimate moment capacity [24].

## 5. Material constitutive laws

### *5.1. Structural steels*

The steel tubes in CFDST columns are subjected to biaxial stresses which reduce their yield strength in the longitudinal direction. The stress and strain relationships of structural steel material are given in Fig. 16, where $\sigma_s$ and $\varepsilon_s$ are the longitudinal stress and strain in steel, respectively; $\varepsilon_{st}$ and $\varepsilon_{su}$ are the strains at the onset of strain-hardening and at the ultimate strain,

and taken as 0.005 and 0.2, respectively. Liang [24] suggested that a reduction factor of 0.9 should be used to reduce the steel yield strength shown in Fig. 16 to consider the effects of biaxial stresses on the steel tube. The formulas to calculate the rounded-part in the stress-strain curve was also suggested by Liang [24] for cold-formed steed while the expression provided by Mander [28] is employed to determine the stresses in the range of strain hardening.

### *5.2. Concrete*

The current and existing test results [6-9] indicate that the effective confinement provided by the circular steel tube significantly increases the ductility as well as the strength of CFDST columns composed of circular tubes. Moreover, the results obtained from finite element analyses presented by Chang et al. [2] confirmed that longitudinal stress in sandwiched concrete was similar to the concrete in circular CFST columns while the core-concrete in a circular CFDST column loaded was subjected to a higher compressive longitudinal stress than the sandwiched-concrete. When the compressive load increases, the sandwiched-concrete and the core-concrete expand more than the steel tubes, the external steel tube confines the sandwiched-concrete. The sandwiched-concrete under lateral compression exerts lateral pressure on the internal steel tube which therefore confines the core-concrete. Therefore, it can be assumed that the sandwiched-concrete is mainly confined by the external tube while the core-concrete is effectively confined by both the external and internal tubes in a circular CFDST column [1-3]. Ahmed et al. [1] proposed constitutive laws of confined concrete in circular CFDST columns. The two-stage stress and strain curves for unconfined and confined concrete illustrated in Fig. 17 was originally derived by Lim and Ozbakkaloglu [29]. A general stress-strain model is adopted for both sandwiched-concrete and core-concrete, but different lateral confining pressure models are used to determine the confinement on the sandwiched-concrete and ore-

concrete. The ascending branch of the curves is expressed by the equations presented by Mander et al. [30] as

$$\sigma_c = \frac{f_{cc}^{'}(\varepsilon_c / \varepsilon_{cc}^{'})\lambda}{(\varepsilon_c / \varepsilon_{cc}^{'})^{\lambda} + \lambda - 1} \tag{5}$$

$$\lambda = \frac{\varepsilon_{cc}^{'} E_c}{\varepsilon_{cc}^{'} E_c - f_{cc}^{'}} \tag{6}$$

in which $\sigma_c$ and $\varepsilon_c$ denote the longitudinal stress and the corresponding strain; $f_{cc}^{'}$ and $\varepsilon_{cc}^{'}$ represent the maximum strength of compressive concrete and its corresponding strain, respectively; $E_c$ is the modulus of elasticity of concrete, calculated as [23]

$$E_c = 4400\ \sqrt{\gamma_c\, f_c'}\ \text{(MPa)} \tag{7}$$

in which $\gamma_c = 1.85 D_c^{-0.135}$ is the reduction factor applied to the concrete compressive strength taking into account the column size effect, in which $D_c$ stands for the concrete-core diameter and is $(D_i - 2t_i)$ for core-concrete and $(D_o - 2t_o)$ for sandwiched concrete.

The confinement is explicitly taken into account in the stress-strain model for confined concrete. As shown in Fig. 4, the confinement effect is included when the compressive stress in the concrete fibers is greater than $\gamma_c f_c^{'}$. The confinement increases the concrete compressive strength from $\gamma_c f_c^{'}$ to the maximum value of $f_{cc}^{'}$. The maximum compressive strength ( $f_{cc}^{'}$ ) together with the corresponding strain ( $\varepsilon_{cc}^{'}$ ) are calculated as

$$f_{cc}^{'} = \gamma_c f_c^{'} + 4.1 f_{rp} \tag{8}$$

$$\varepsilon_{cc}^{'} = \varepsilon_c^{'} + \frac{20.5 f_{rp} \varepsilon_c^{'}}{\gamma_c f_c^{'}} \tag{9}$$

where $f_{rp}$ generally defines the lateral pressure on the confined concrete. For the sandwiched concrete, the lateral pressure ( $f_{rpo}$ ) is calculated by the equation proposed by Hu et al. [19] as

$$\frac{f_{rpo}}{f_{syo}} = \begin{cases} 0.043646 - 0.000832\left(\frac{D_o}{t_o}\right) & \text{for } 21.7 \le \frac{D_o}{t_o} \le 47 \\ 0.006241 - 0.0000357\left(\frac{D_o}{t_o}\right) & \text{for } 47 < \frac{D_o}{t_o} \le 150 \end{cases} \tag{10}$$

in which $f_{syo}$ is the yield strength of the outer steel tube.

Based on the test results, Ahmed et al. [1] proposed an equation for estimating the lateral pressure on the core-concrete ( $f_{rpi}$ ) in CFDST columns, expressed as

$$f_{rpi} = 2.2897 + 0.0066\left(\frac{D_o}{t_o}\right) - 0.1918\left(\frac{D_i}{t_i}\right) - \left[0.0585\left(\frac{D_o}{t_o}\right) - 0.3801\left(\frac{D_i}{t_i}\right)\right]\zeta^{-1} \quad \left(f_{rpi} \ge 0\right) \tag{11}$$

in which the confinement factor $\zeta$ is defined as

$$\zeta = \frac{A_{so} f_{sy,o} + A_{si} f_{sy,i}}{A_{sc}\gamma_c f_{sc}^{'} + A_{cc}\gamma_c f_{cc}^{'}} \tag{12}$$

The strain ($\varepsilon_c^{'}$) corresponding to the maximum strength $f_c^{'}$ of the unconfined compressive concrete shown in Fig. 17 is calculated using the expression given by De Nicolo et al. [31] as

$$\varepsilon_c^{'} = 0.00076 + \sqrt{(0.626\gamma_c f_c^{'} - 4.33)\times 10^{-7}} \tag{13}$$

Lim and Ozbakkaloglu [29] proposed an equation to express the descending branch of stress-strain curves as

$$\sigma_c = f_{cc}^{'} - \frac{f_{cc}^{'} - f_{cr}}{\left[1+\left(\frac{\varepsilon_c - \varepsilon_{cc}^{'}}{\varepsilon_{ci} - \varepsilon_{cc}^{'}}\right)^{-2}\right]} \tag{14}$$

where $f_{cr}$ is the residual strength of concrete, which was proposed by Ahmed et al. [1] as

$$\frac{f_{cr}}{f_{cc}^{'}} = 1.2420 - 0.0029\left(\frac{D}{t}\right) - 0.0044\,\gamma_c f_c^{'} \qquad \left(0 \le \frac{f_{cr}}{f_{cc}^{'}} \le 1.0\right) \tag{15}$$

The original equation developed by Lim and Ozbakkaloglu [29] for calculating the strain at the inflection point ($\varepsilon_{ci}$) is modified to consider the column size effects as

$$\varepsilon_{ci} = 2.8\varepsilon_{cc}^{'}\left(\gamma_c f_c^{'}\right)^{-0.12}\left(\frac{f_{cr}}{f_{cc}^{'}}\right) + 10\varepsilon_{cc}^{'}\left(\gamma_c f_c^{'}\right)^{-0.47}\left(1 - \frac{f_{cr}}{f_{cc}^{'}}\right) \tag{16}$$

The relationships of stress and strain of concrete in tension are illustrated in Fig. 17, where $f_{\alpha}$ and $\varepsilon_{tc}$ are the tensile strength and corresponding strain of concrete. The ultimate strength ($f_{\alpha}$)

of concrete in tension is specified as $0.6\sqrt{\gamma_c f_c'}$ and the corresponding strain $\varepsilon_{tu}$ is determined as ten times the cracking strain.

## 6. Experimental verification

The accuracy of the mathematical modeling technique proposed is assessed by means of comparing the predicted strength envelopes with experimental results in Fig. 18. The experimental ultimate moment ($M_{u,\exp}$) was determined as the product of the ultimate axial load ($P_{u,\exp}$) and eccentricity ($e$). It can be observed from the comparisons that the computational results are generally in good agreement with measurements. However, the ultimate loads of CFDST columns under concentric loads are slightly underestimated by the numerical model and experimental ultimate moments of Columns CC7 and CC12 are slightly lower than the predicted values. The uncertainty in the actual concrete strengths in the tested specimens may cause these discrepancies as the average compressive strengths of concrete were specified in the numerical analyses. The difference between the experimental and predicted ultimate moments of Columns CC9, CC14 and CC19 is caused by the failure of the column ends subjected to large loading eccentricities as shown in Fig. 8.

The computational model proposed has been further developed to simulate the load-deflection responses of circular CFDST short and slender columns loaded eccentrically [26]. The accuracy of the computational model is validated by comparing the calculations with the measured load-deflection curves of eccentrically loaded circular CFDST short and slender columns tested by the authors and Ibañez et al. [11]. The initial eccentricity of the tested short columns was taken as $L$/650 in the numerical analyses. It would appear from Figs. 19 that reasonable agreement between test data and numerical results for short CFDST columns is obtained. The difference

between experiments and computations is likely attributed to the uncertainty in the actual strengths of concrete in the tested columns. Moreover, as the concrete strength is very low, the concrete model adopted might not accurately capture the behavior of low strength concrete. However, the numerical model predicts well the complete load-deflection curves of slender CFDST columns as depicted in Fig. 20. This approves that the mathematical model proposed can accurately predict the structural behavior of circular CFDST columns loaded eccentrically.

## 7. Parametric studies

The mathematical model, which was implemented in a computer program, was employed to examine the sensitivities of moment-curvature responses and strength envelopes of CFDST columns composed circular sections to various important design parameters. The stress-strain model for concrete in circular CFDST columns has been verified by experimental results by the authors [1], and can be used to model the material behavior of both normal and high strength concrete in CFDST columns. For practical applications, the concrete strength used in CFDST columns is usually above 40 MPa. Therefore, the concrete strengths varying from 40 MPa to 100 MPa were used in the parametric studies. The following data were used for the reference column: $D_o = 450$ mm, $t_o = 10$ mm, $D_i$ =200 mm, $t_i$ =6.67 mm, $f_{syo} = f_{syi} = 350$ MPa, $E_s$ = 200 GPa, the concrete strength of the sandwiched-concrete and the core-concrete was taken as $f_{co}^{'} = f_{ci}^{'} = 70$ MPa, and the load ratio was specified as $P_u/P_o$ =0.4.

### *7.1. $D_o / t_o$ ratio*

The effects of the ratio of $D_o / t_o$ on the structural behavior of CFDST circular columns were examined by utilizing the computational model developed. The $D_o / t_o$ ratio of CFDST

columns was varied from 35 to 45, 55 and 65 by altering the thickness of the external tube only. The moment-curvature curves and strength envelopes of CFDST columns are presented in Figs. 21 and 22, respectively. Under the constant axial load of 6591 kN, increasing ratio of $D_o / t_o$ remarkably reduces both the initial bending stiffness and resistance of CFDST columns as demonstrated in Fig. 21. This is caused by the decrease in the steel area of the outer tube. The ultimate moment capacity is decreased by 35.7% by increasing the ratio $D_o / t_o$ from 35 to 65. Moreover, Fig. 22 indicates that the ratio $D_o / t_o$ has a considerable influence on the pure ultimate axial and the pure bending moment. Changing the $D_o / t_o$ ratio from 35 to 45, 55 and 65 causes an increase in the pure ultimate axial strength of the columns by 13.7%, 19.6% and 22.5%, respectively, while the increases in the pure bending resistance were calculated as 18.1%, 29.2% and 36.69%, respectively.

### *7.2. $D_i / t_i$ ratio*

The sensitivities of the structural responses of circular CFDST columns to the ratio $D_i / t_i$ were examined by altering the thickness of the inner tube only. The moment-curvature relations of CFDST columns under a constant axial load of 6591 kN are given in Fig. 23. It is observed that the ratio $D_i / t_i$ has a minor effect on the moment-curvature behavior of the CFDST columns. The bending resistance of the CFDST columns decreases by only 0.3% when the ratio $D_i / t_i$ increases from 30 to 60. The curvature ductility index of CFDST columns having the $D_i / t_i$ ratio of 30 is 18.13 but it is 15.11 for the CFDST column having the $D_i / t_i$ ratio of 60. The strength curves generated by the computational model are given in Fig. 24. It is apparent that the influence of the $D_i / t_i$ ratio on the strength envelopes is insignificant. The decreases in the

pure ultimate axial and the bending strengths are only 2.3% and 5.2%, respectively when the ratio $D_i / t_i$ is changed from 30 to 60.

### *7.3. $D_i / D_o$ ratio*

The diameter of the inner tube was changed to investigate the significance of the ratio $D_i / D_o$ on the responses of CFDST columns. The moment-curvature curves for the columns that were loaded by a constant axial load of 6591 kN are given in Fig. 25. It is evident that increasing the ratio $D_i / D_o$ slightly increases the initial bending stiffness but improves the ultimate bending strength of CFDST columns considerably. When the ratio $D_i / D_o$ is changed from 0.33 to 0.44, 0.55 and 0.66, the column ultimate moment increases by 4.7%, 11.9% and 21.6%, respectively. The curvature ductility index of CFDST columns increases from 20.1 to 23.3 by changing the ratio $D_i / D_o$ from 0.33 to 0.66. The computed strength envelopes of CFDST columns have been drawn in Fig. 26. The change of the $D_i / D_o$ ratio from 0.33 to 0.66 improves the pure ultimate axial load by 15% and the pure ultimate moment of the CFDST column by 15.1%.

### *7.4. Steel yield strength*

The steel yield stress of circular CFDST columns was varied from 250 MPa to 550 MPa to ascertain its influences on their structural performance. The influences of steel yield stress on the moment-curvature behavior of the CFDST columns subjected to the constant axial load of 6591 kN are shown in Fig. 27. It would appear from Fig. 27 that the initial bending stiffness of the columns is appreciably improved by using the steel tubes with higher yield stress. Changing the steel yield stress from 250 MPa to 650 MPa causes a marked increase in the ultimate

moment by70.8%. However, the column ductility index reduces from 17.89 to 14.11 when the steel tubes with the yield stress of 650 MPa are used instead of those with the yield stress of 250 MPa. The sensitivity of the interaction behavior to the steel yield stress is demonstrated in Fig. 28. The figure indicates that the higher the yield stress of the steel tubes, the higher the pure ultimate axial and bending strengths of the column. However, the steel yield stress has the most pronounced impact on the pure bending moment. The pure ultimate axial and pure bending strengths increase by 38.7% and 90.4%, respectively when changing the steel yield stress from 250 MPa to 650 MPa.

### *7.5. Concrete compressive strength*

The sensitivities of the moment-curvature and strength interaction responses of CFDST columns to the concrete compressive strengths varied from 40 MPa to 100 MPa were examined. The simulated moment-curvature curves for the columns loaded by the constant axial load of 6591 kN are given in Fig. 29. The column's initial bending stiffness has a marked improvement due to the increase in the concrete compressive strength. Changing the concrete strength from 40 MPa to 100 MPa increases the ultimate moment capacity of the column by 37.5%, however, its ductility index decreases from 18.67 to 9.01. Figure 30 shows that the concrete strength has a greater effect on the pure ultimate axial load of the CFDST column than on its pure bending moment. As a result of increasing the concrete strength from 40 MPa to 100 MPa, the pure ultimate axial load increases by 51.7% while the pure ultimate moment increases only 8.9%.

### *7.6. Concrete confinement*

The concrete confinement is an important feature that has a remarkable effect on the responses

of circular CFDST columns loaded eccentrically. The computer program developed was employed to ascertain this effect. The thickness $t_o$ of the reference column was changed to produce a $D_o / t_o$ ratio of 100 while $D_i$ was changed to $D_i = D_o / 3$. The other parameters of the reference column remained the same. The moment-curvature and interaction strength curves of the CFDST column with and without considering the confinement effect are provided in Figs. 31 and 32, respectively. It is discovered that ignoring the confinement effect considerably underestimates the performance of the CFDST column. When the confinement is not considered in the numerical modeling, the column ultimate and residual moment capacity is underestimated by 13.4% and 37% as indicated in Fig. 31. Moreover, the confinement has a considerable influence on the interaction curves of CFDST columns as demonstrated in Fig. 32. If the confinement is not considered in the simulation, the pure ultimate axial load of the columns is underestimated by 7.4% while the pure bending moment is underestimated by 1.1%.

### *7.7. Axial load ratio*

The computer model was used to ascertain the influences of the applied axial load ratio ($P_u/P_o$) on the responses of CFDST columns. The moment-curvature curves of the CFDST column with the $P_u/P_o$ ratios varied from 0.3 to 0.4, 0.5 and 0.6 are presented in Fig. 33. The initial bending stiffness and moment capacity are markedly decreased by increasing the load ratio. However, this effect is more significant for the $P_u/P_o$ ratio larger than 0.5. If the axial load ratio is changed from 0.3 to 0.4 and 0.5, the bending resistance of the CFDST column decreases by only 2.5% and 8.7%, respectively. However, when the $P_u/P_o$ ratio increases from 0.3 to 0.6, the ultimate moment reduces by 18.7%. The ductility performance of the CFDST column is insignificantly influenced by the $P_u/P_o$ ratio as indicated in Fig. 33.

### *7.8. Moment distributions in CFDST columns*

The moment distributions in circular CFDST columns loaded eccentrically have not been investigated. To provide information on the moment distributions, the circular CFDST beam-column that had the following geometric and material properties was analyzed by the computational model: $D_o = 800$ mm, $t_o = 8$ mm, $D_i$ =400 mm, $t_i$ =8 mm, $f_{syo} = f_{syi} = 350$ MPa, $E_s = 200$ GPa and $f_{co}^{'} = f_{ci}^{'} = 50$ MPa. In the moment-curvature analysis, the axial load of 22289 kN was applied to the beam-column. The predicted moment distributions in the external steel tube, inner steel tube, sandwiched concrete and core-concrete as a function of the curvature are schematically presented in Fig. 34, where the moment-curvature curve for the CFDST column is also shown. At the maximum moment, the moments carried by the external steel tube, the sandwiched concrete, the core-concrete and the internal steel tube were calculated as 48.7%, 32.1%, 10.6% and 8.6%, respectively. The results indicate that the external steel tube and sandwiched-concrete withstand a large portion of the ultimate moment. The reason for this is that the sandwiched-concrete and external steel tube have larger cross-sectional areas and are located farer from the section centroid than the internal steel tube and core concrete.

## 8. Conclusions

This paper has described experimental and computational investigations into the behavior of CFDST short columns composed of circular tubes that are axially and eccentrically loaded. The experimental results have been employed to verify the computer modeling technique developed for quantifying the moment-curvature and strength interaction behavior of circular CFDST columns incorporating concrete confinement effects. Parametric studies on the structural responses of CFDST columns including various important features have been conducted.

Experiments conducted indicate that the local buckling of the internal steel tube is effectively prevented by the rigid concrete and the core-concrete in circular CFDST columns does not crush due to the confinement provided by the steel tubes. The experimental data on circular CFDST short columns under eccentric loading presented in this paper for the first time can be used to validate other numerical models. The fiber-based computational method proposed is shown to be efficient and accurate, and can be employed to analyze and design of CFDST beam-columns in practice. Numerical results presented on the moment-curvature responses, strength envelopes, concrete confinement effect, and moment distributions in circular CFDST short columns loaded eccentrically provide a better understanding of the fundamental behavior of CFDST columns. It has been demonstrated that the outer steel tube carries the largest portion of the moment followed by the sandwiched concrete while the core-concrete and inner steel tube make less contributions to the moment capacity of the CFDST column.

**Acknowledgements**

The experimental work discussed in this paper was financially supported by both Victoria University and La Trobe University, Australia. The financial support is gratefully acknowledged. The authors thank the technicians at both Victoria University and the University of Wollongong, Australia for their technical support, particularly Mr. Ritchie McLean and Mr. Duncan Best in the structure laboratory at the University of Wollongong, Australia for their helpful assistance during the experiments.

## References

[1] M. Ahmed, Q. Q. Liang, V. I. Patel, M. N. S. Hadi, Numerical analysis of axially loaded circular high strength concrete-filled double steel tubular short columns, Thin-Walled Struct. 138 (2019) 105-116.

[2] X. Chang, Z. L. Ru, W. Zhou, Y. B. Zhang, Study on concrete-filled stainless steel–carbon steel tubular (CFSCT) stub columns under compression, Thin-Walled Struct. 63 (2013) 125-133.

[3] M. F. Hassanein, O. F. Kharoob, Q. Q. Liang, Behaviour of circular concrete-filled lean duplex stainless steel–carbon steel tubular short columns, Eng. Struct. 56 (2013) 83-94.

[4] Eurocode 4, Design of composite steel and concrete structures-Part 1-1: General rules and rules for buildings, European Committee for Standardization, CEN, Brussels, Belgium, 2004.

[5] ANSI/AISC 360-16, Specification for Structural Steel Buildings, American Institute of Steel Construction, Chicago, IL, 2016.

[6] M. X. Xiong, D. X. Xiong, J. Y. R. Liew, Axial performance of short concrete filled steel tubes with high-and ultra-high-strength materials, Eng. Struct. 136 (2017) 494-510.

[7] Y. Y. Peng, K. F. Tan, Y. Yao, Mechanical properties of duplex steel tube high- strength concrete short columns under axial compression, J. Wuhan Univ. Tech. 33 (2) (2011) 105-109 (In Chinese).

[8] C. Y. Wan, X. X. Zha, Nonlinear analysis and design of concrete-filled dual steel tubular columns under axial loading, Steel and Compo. Struct. 20 (3) (2016) 571-597.

[9] T. Ekmekyapar, B. J. Al-Eliwi, Concrete filled double circular steel tube (CFDCST) stub columns, Eng. Struct. 135 (2017) 68-80.

[10] M. L. Romero, A. Espinós, J. Portolés, A. Hospitaler, C. Ibañez, Slender double-tube ultra-high strength concrete-filled tubular columns under ambient temperature and fire, Eng. Struct. 99 (2015) 536-545.

[11] C. Ibañez, M. L. Romero, A. Espinós, J. M. Portolés, V. Albero, Ultra-high strength concrete on eccentrically loaded slender circular concrete-filled dual steel columns, Struct. 12 (2017) 64-74.

[12] Y. Zheng, C. He, L. Zheng, Experimental and numerical investigation of circular double-tube concrete-filled stainless steel tubular columns under cyclic loading, Thin-Walled Struct. 132 (2018) 151-166.

[13] V. I. Patel, Q. Q. Liang, M. N. S. Hadi, Nonlinear analysis of axially loaded circular concrete-filled stainless steel tubular short columns, J. Constr. Steel Res. 101 (2014) 9-18.

[14] V. I. Patel, Q. Q. Liang, M. N. S. Hadi, Concrete-filled stainless steel tubular columns.CRC Press, Taylor and Francis, Boca Raton and London, 2018.

[15] Y. Zheng, Z. Tao, Compressive strength and stiffness of concrete-filled double-tube columns, Thin-Walled Struct. 134 (2019) 174-188.

[16] M. F. Hassanein, M. Elchalakani, V. I. Patel, Overall buckling behaviour of circular concrete-filled dual steel tubular columns with stainless steel external tubes, Thin-Walled Struct. 115 (2017) 336-348.

[17] U. Katwal, Z. Tao, M. K. Hassan, W. D. Wang, Simplified numerical modeling of axially loaded circular concrete-filled steel stub columns, J. Struct. Eng. ASCE, 143 (12) (2017) 04017169.

[18] Z. Tao, Z.-B. Wang, Q. Yu, Finite element modelling of concrete-filled steel stub columns under axial compression, J. Constr. Steel Res. 89 (2013) 121-131.

[19] H. T. Hu, C. S. Huang, M. H. Wu, Y. M. Wu, Nonlinear analysis of axially loaded concrete-filled tube columns with confinement effect, J. Struct. Eng. 129 (10) (2003) 1322-1329.

[20] AS 1391-2007. Metallic materials - Tensile testing at ambient temperature, Standards Australia, Sydney, NSW, Australia, 2007.

[21] M. N. S. Hadi, I. B. R. Widiarsa, Axial and flexural performance of square RC columns wrapped with CFRP under eccentric loading, J. Compo. Constr. 16 (6) (2012) 640-649.

[22] M. Ahmed, Q. Q. Liang, V. I. Patel, M. N. S. Hadi, Nonlinear analysis of rectangular concrete-filled double steel tubular short columns incorporating local buckling, Eng. Struct. 175 (2018) 13-26.

[23] Q. Q. Liang, Nonlinear analysis of circular double-skin concrete-filled steel tubular columns under axial compression, Eng. Struct. 131 (2017) 639-650.

[24] Q. Q. Liang, Performance-based analysis of concrete-filled steel tubular beam–columns, Part I: Theory and algorithms, J. Constr. Steel Res. 65 (2) (2009) 363-372.

[25] V. I. Patel, Q. Q. Liang, M. N. S. Hadi, Nonlinear analysis of concrete-filled steel tubular columns, Scholar's Press, Germany, 2015.

[26] M. Ahmed, Q. Q. Liang, V. I. Patel, M. N. S. Hadi, Local-global interaction buckling of square high strength concrete-filled double steel tubular slender beam-columns, Thin-Walled Struct. 143 (2019) 106244.

[27] M. Ahmed, Q. Q. Liang, V. I. Patel, M. N. S. Hadi, Experimental and numerical studies of square concrete-filled double steel tubular short columns under eccentric loading, Eng. Struct. 143 (2019) 109419.

[28] J. B. Mander, Seismic design of bridge piers, (Ph.D. Thesis), Christchurch, New Zealand, Dep. Civ. Eng., Uni. Cant., 1983.

[29] J. C. Lim, T. Ozbakkaloglu, Stress–strain model for normal-and light-weight concretes under uniaxial and triaxial compression, Const. Build. Mat. 71 (2014) 492-509.

[30 J. B. Mander, M. J. Priestley, R. Park, Theoretical stress-strain model for confined concrete, J. Struct. Eng. 114 (8) (1988) 1804-1826.

[31] B. De Nicolo, L. Pani, E. Pozzo, Strain of concrete at peak compressive stress for a wide range of compressive strengths, Mat. Struct. 27 (4) (1994) 206-210.

## Figures and tables

**Table 1** Geometric and material properties of circular CFDST short columns.

| Group | Column | Length $L$ (mm) | Outer tube | | Inner tube | | $f_c'$ (MPa) | $e$ (mm) | $e/D_o$ | $P_{u,\exp}$ (kN) |
|---|---|---|---|---|---|---|---|---|---|---|
| | | | $D_o \times t_o$ (mm) | $\frac{D_o}{t_o}$ | $D_i \times t_i$ (mm) | $\frac{D_i}{t_i}$ | | | | |
| G1 | CC1 | 420 | 139.7× 5.0 | 27.9 | 76.1×3.6 | 21.1 | 19.1 | 0 | 0 | 1605 |
| | CC2 | 420 | 139.7× 5.0 | 27.9 | 76.1×3.6 | 21.1 | 19.1 | 10 | 0.07 | 1268 |
| | CC3 | 420 | 139.7× 5.0 | 27.9 | 76.1×3.6 | 21.1 | 19.1 | 25 | 0.18 | 951 |
| | CC4 | 420 | 139.7× 5.0 | 27.9 | 76.1×3.6 | 21.1 | 19.1 | 30 | 0.21 | 871 |
| G2 | CC5 | 495 | 165.1× 5.0 | 33.0 | 88.9×4.0 | 22.2 | 19.1 | 0 | 0 | 1721 |
| | CC6 | 495 | 165.1× 5.0 | 33.0 | 88.9×4.0 | 22.2 | 19.1 | 0 | 0 | 1717 |
| | CC7 | 495 | 165.1× 5.0 | 33.0 | 88.9×4.0 | 22.2 | 19.1 | 10 | 0.06 | 1327 |
| | CC8 | 495 | 165.1× 5.0 | 33.0 | 88.9×4.0 | 22.2 | 19.1 | 20 | 0.12 | 1184 |
| | CC9 | 495 | 165.1× 5.0 | 33.0 | 88.9×4.0 | 22.2 | 19.1 | 35 | 0.21 | 893 |
| G3 | CC10 | 420 | 139.7× 3.5 | 39.9 | 76.1×3.2 | 23.8 | 20.6 | 0 | 0 | 1491 |
| | CC11 | 420 | 139.7× 3.5 | 39.9 | 76.1×3.2 | 23.8 | 20.6 | 0 | 0 | 1489 |
| | CC12 | 420 | 139.7× 3.5 | 39.9 | 76.1×3.2 | 23.8 | 20.6 | 10 | 0.07 | 1023 |
| | CC13 | 420 | 139.7× 3.5 | 39.9 | 76.1×3.2 | 23.8 | 20.6 | 20 | 0.14 | 918 |
| | CC14 | 420 | 139.7× 3.5 | 39.9 | 76.1×3.2 | 23.8 | 20.6 | 30 | 0.21 | 765 |
| G4 | CC15 | 495 | 165.1× 3.5 | 47.2 | 88.9×3.2 | 27.8 | 20.6 | 0 | 0 | 1911 |
| | CC16 | 495 | 165.1× 3.5 | 47.2 | 88.9×3.2 | 27.8 | 20.6 | 0 | 0 | 1915 |
| | CC17 | 495 | 165.1× 3.5 | 47.2 | 88.9×3.2 | 27.8 | 20.6 | 10 | 0.06 | 1440 |
| | CC18 | 495 | 165.1× 3.5 | 47.2 | 88.9×3.2 | 27.8 | 20.6 | 20 | 0.12 | 1231 |
| | CC19 | 495 | 165.1× 3.5 | 47.2 | 88.9×3.2 | 27.8 | 20.6 | 35 | 0.21 | 961 |

**Table 2** Material properties of steel tubes obtained from tensile coupon tests.

| Tube type | No. | Geometry of the tube $D \times t$ (mm) | Yield strength, $f_{sy}$ (MPa) | Ultimate strength, $f_{su}$ (MPa) | Yield strain, $\varepsilon_{sy}$ ($\mu\varepsilon$) | Elongation $\Delta$ (%) | Elastic modulus, $E_s$ (GPa) |
|---|---|---|---|---|---|---|---|
| Outer tube | 1 | 139.7× 5.0 | 365 | 449 | 2827 | 20.02 | 210 |
| | 2 | 165.1× 5.0 | 332 | 377 | 3346 | 19.47 | 208 |
| | 3 | 139.7× 3.5 | 412 | 498 | 4368 | 26.53 | 205 |
| | 4 | 165.1× 3.5 | 398 | 510 | 2689 | 26.95 | 196 |
| Inner tube | 1 | 76.1×3.6 | 353 | 398 | 2652 | 17.06 | 205 |
| | 2 | 88.9×4.0 | 345 | 372 | 4156 | 19.28 | 200 |
| | 3 | 76.1×3.2 | 400 | 458 | 1493 | 18.76 | 211 |
| | 4 | 88.9×3.2 | 412 | 471 | 1359 | 20.18 | 200 |

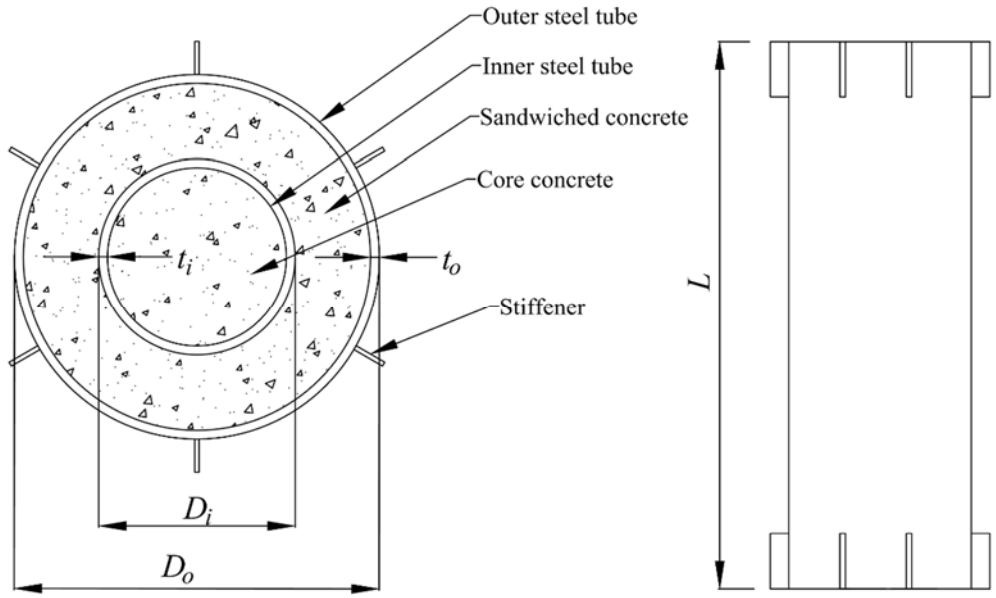


(a) Plan view (b) Elevation view

**Fig. 1.** Schematic view of circular CFDST column.

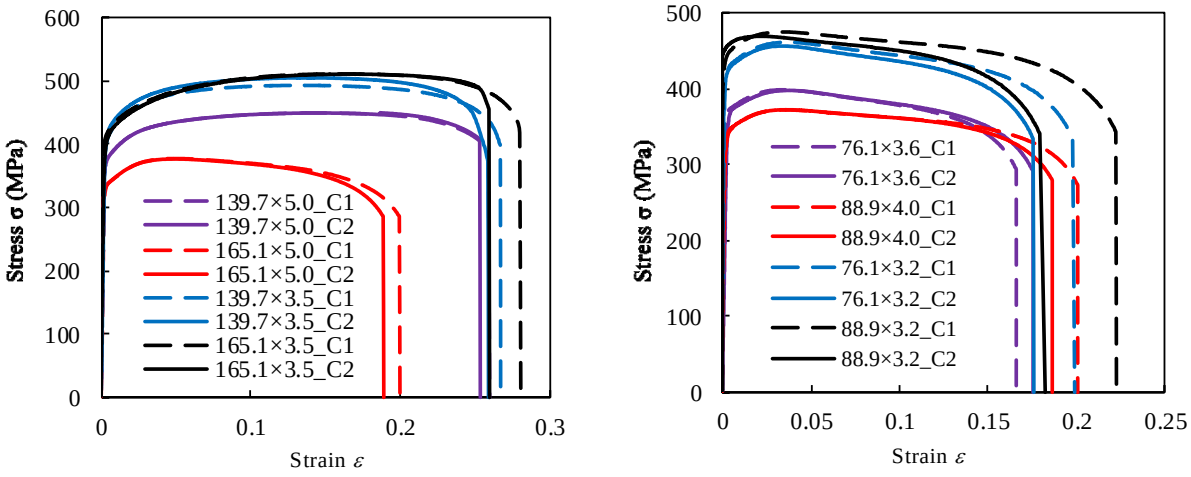


(a) Outer tube (b) Inner tube

**Fig. 2.** Measured stress-strain curves of steel tube materials.


(a) Under axial compression


(b) Under eccentric compression

**Fig. 3.** Test setup of circular CFDST columns.


**Fig. 4.** Failure modes of axially loaded circular CFDST short columns.


**Fig. 5.** Section view of Specimen CC10.

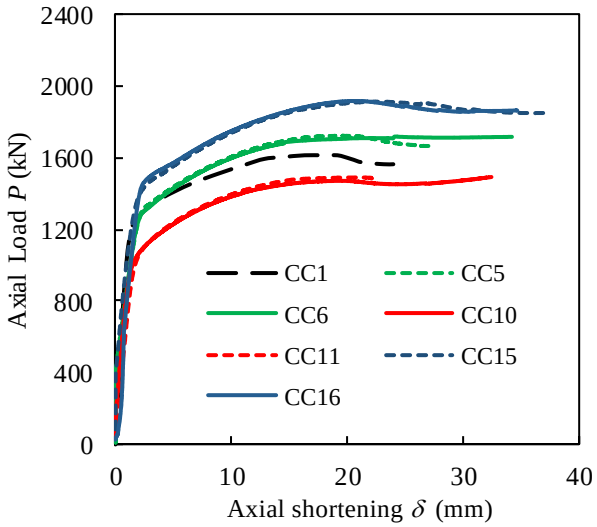


**Fig. 6.** Load-axial shortening curves of circular CFDST short columns under axial compression.

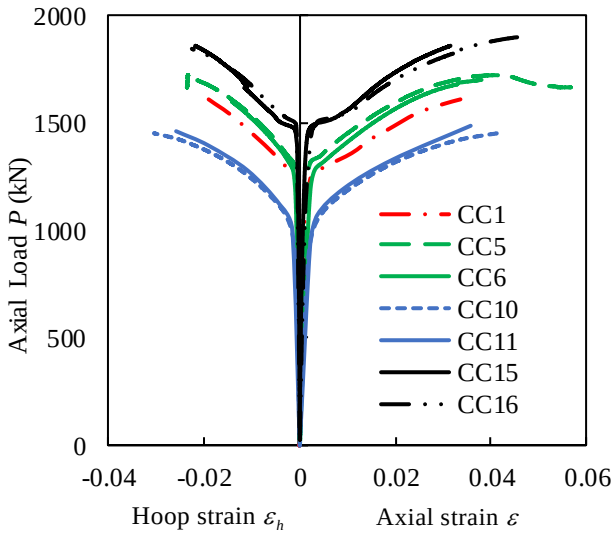


**Fig. 7.** Measured axial load-strain curves of axially loaded circular CFDST short columns.


(a) Group G1


(b) Group G2


(c) Group G3


(d) Group G4

**Fig. 8.** Failure modes of eccentrically loaded circular CFDST short columns.


**Fig. 9.** Separation of sandwiched concrete and inner steel tube of Specimen CC19.


**Fig. 10.** Section view of Specimen CC13.

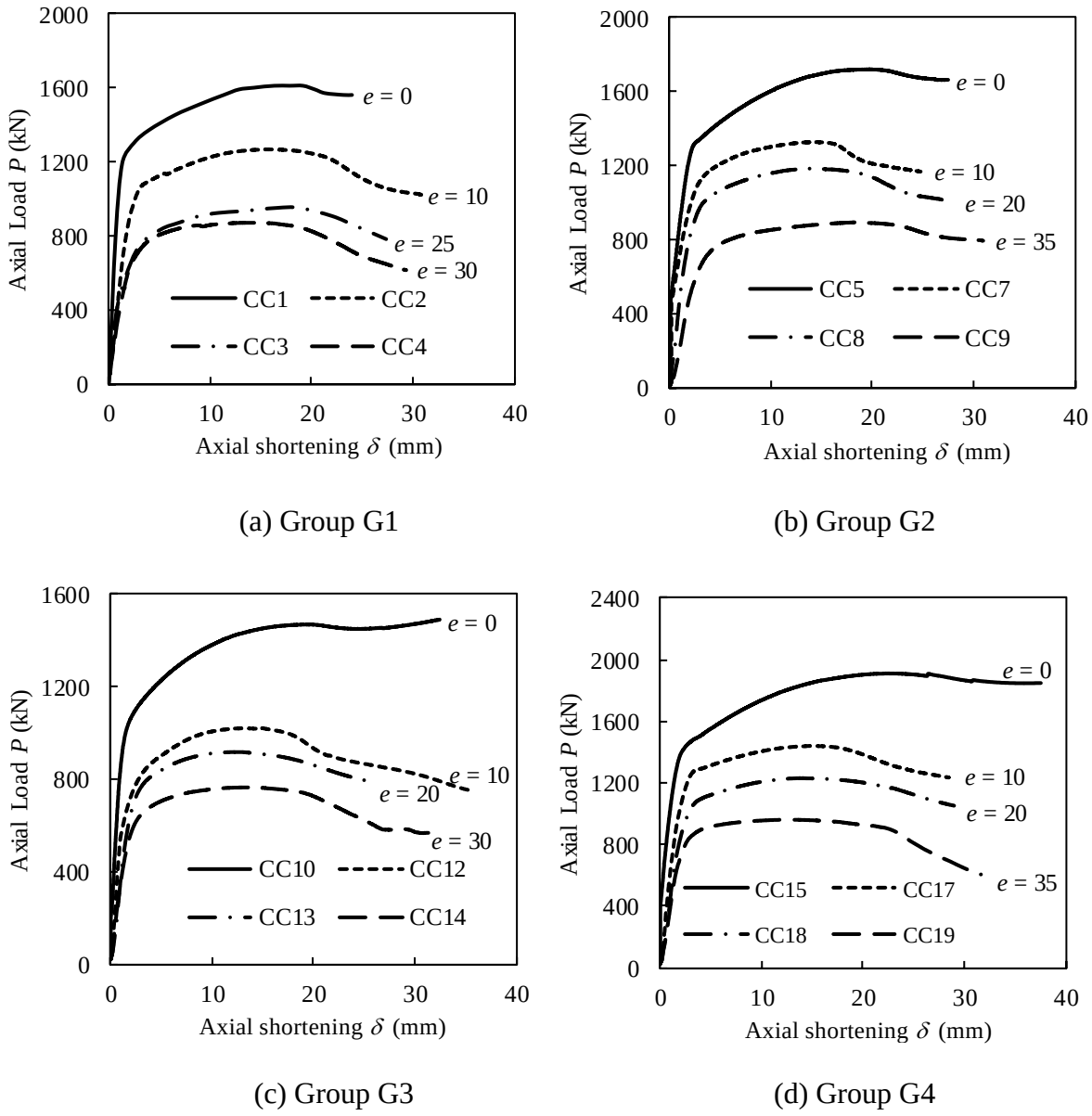


(a) Group G1

(b) Group G2

(c) Group G3

(d) Group G4

**Fig. 11.** Effects of load eccentricity on the axial load-shortening curves of circular CFDST columns.

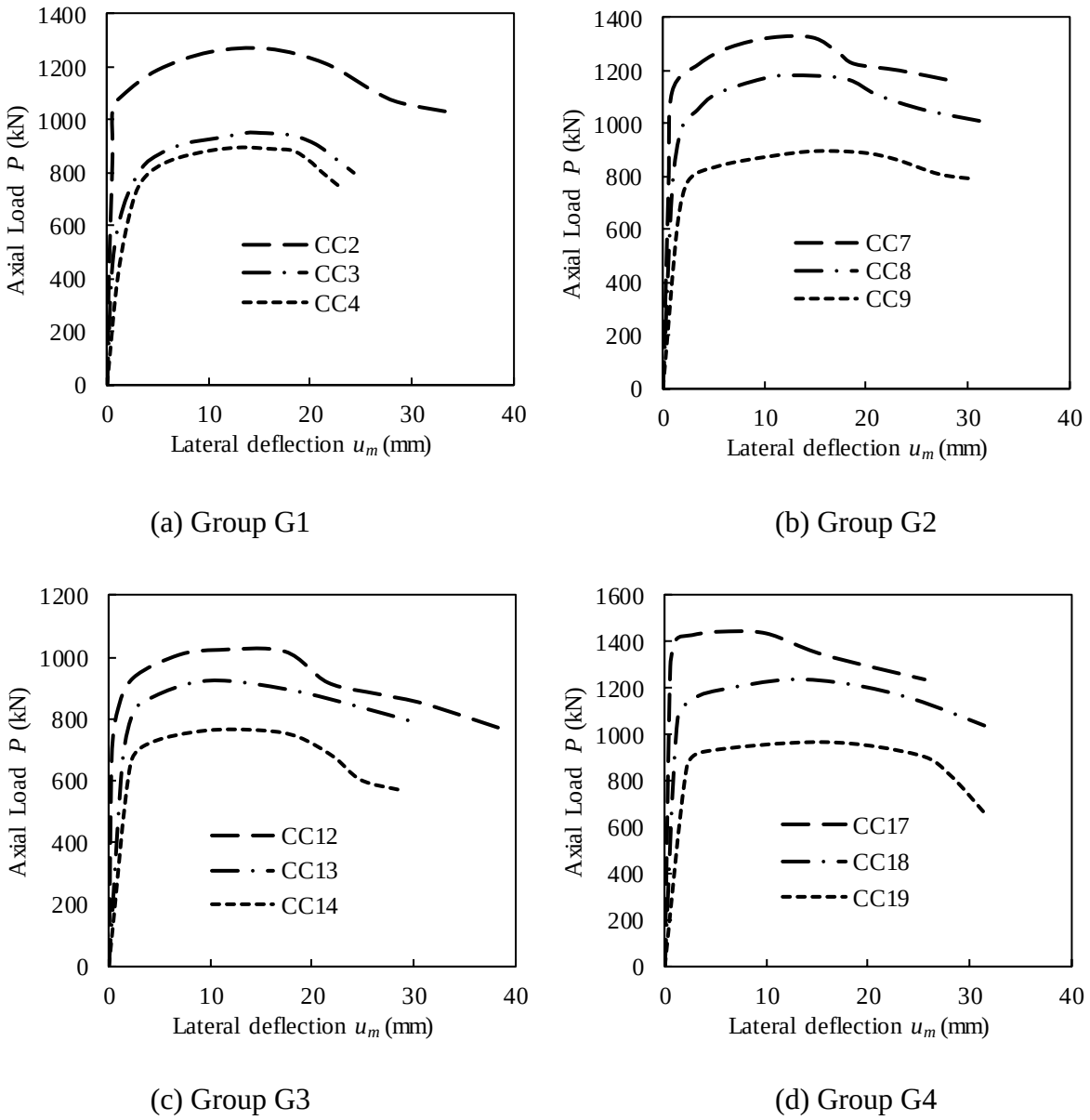


(a) Group G1

(b) Group G2

(c) Group G3

(d) Group G4

**Fig. 12.** Measured axial load-lateral deflection curves of eccentrically loaded circular CFDST columns.

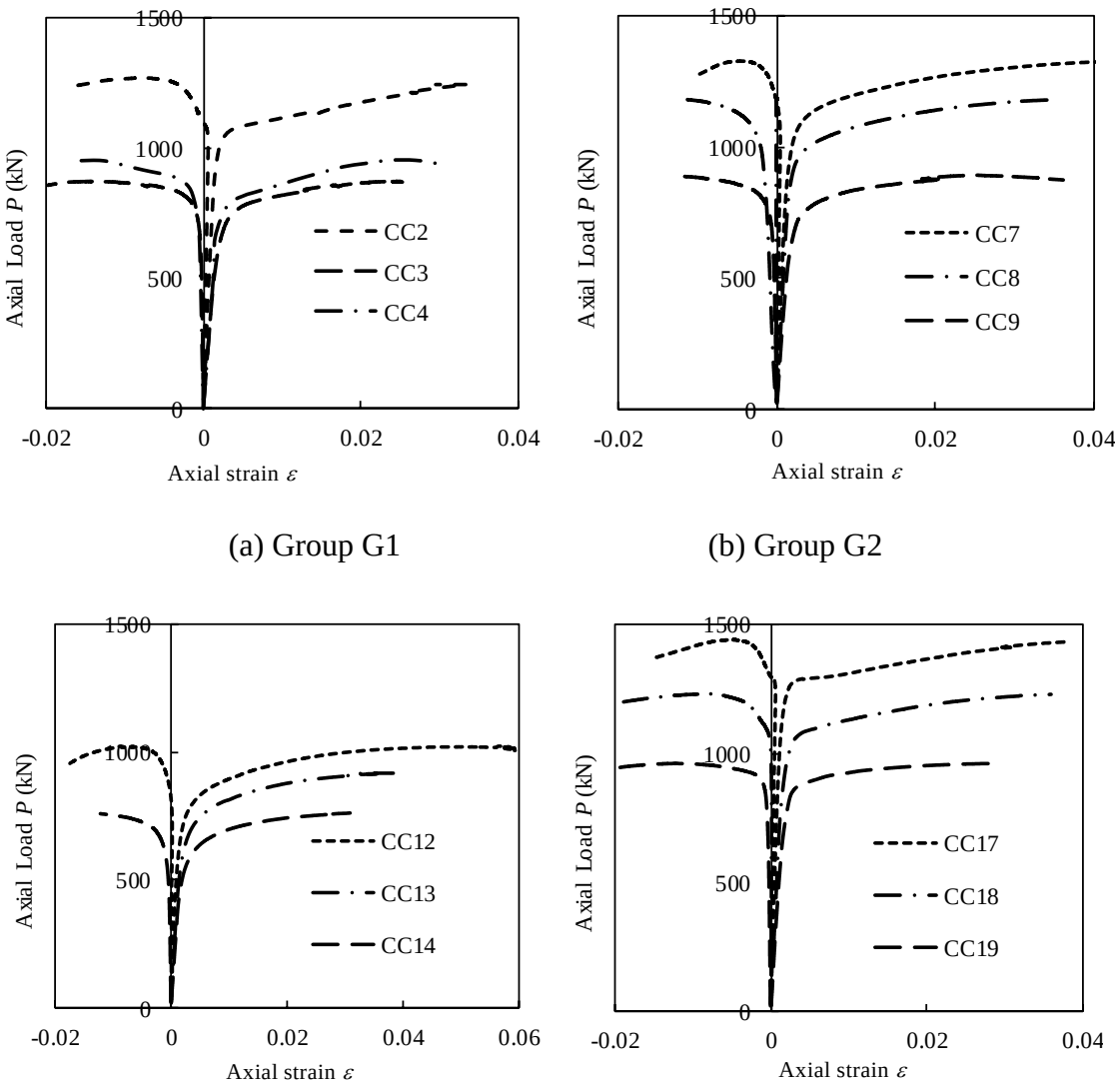


(a) Group G1 (b) Group G2

(c) Group G3 (d) Group G4

**Fig. 13.** Measured load-strain curves of eccentrically loaded circular CFDST short columns.

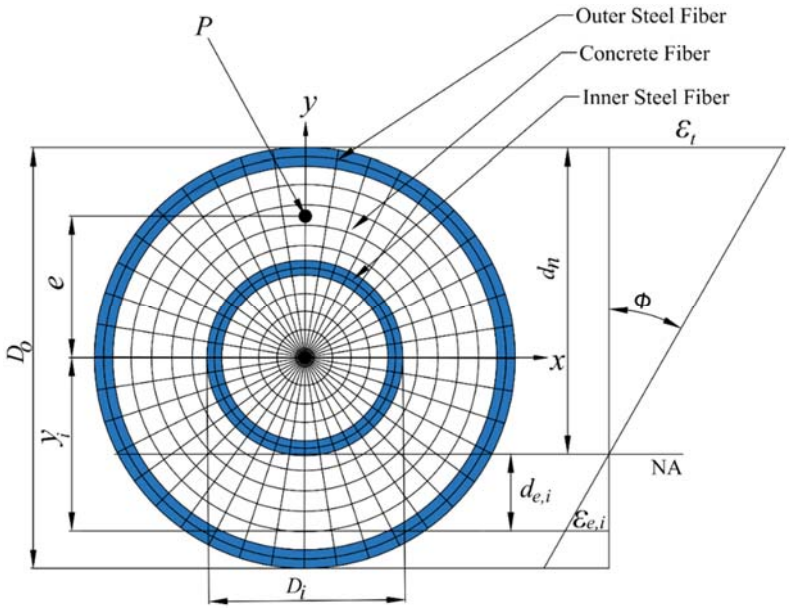


**Fig. 14.** Typical fiber discretization and strain distribution in the cross-section of circular CFDST column.

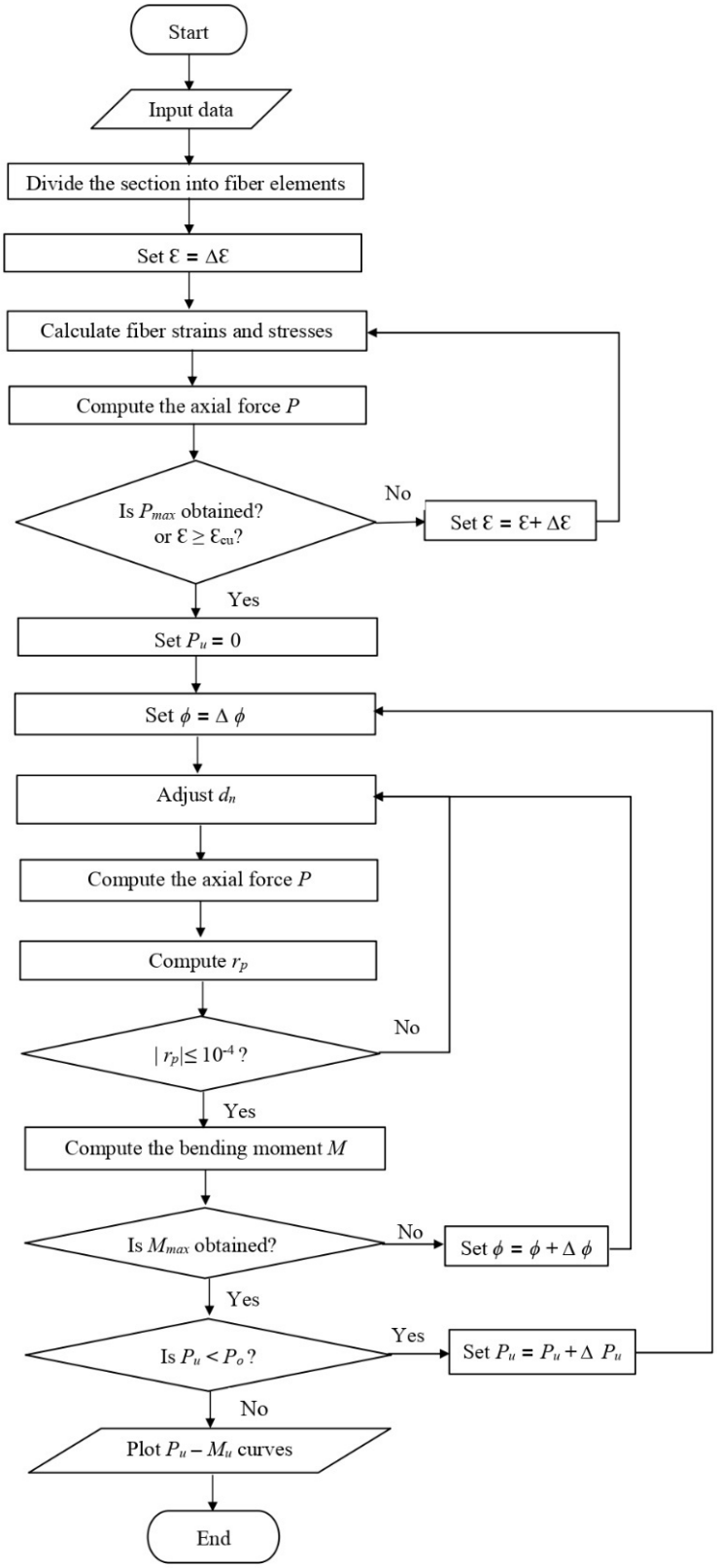


**Fig. 15.** Computer flowchart for calculating axial load-moment interaction curves.

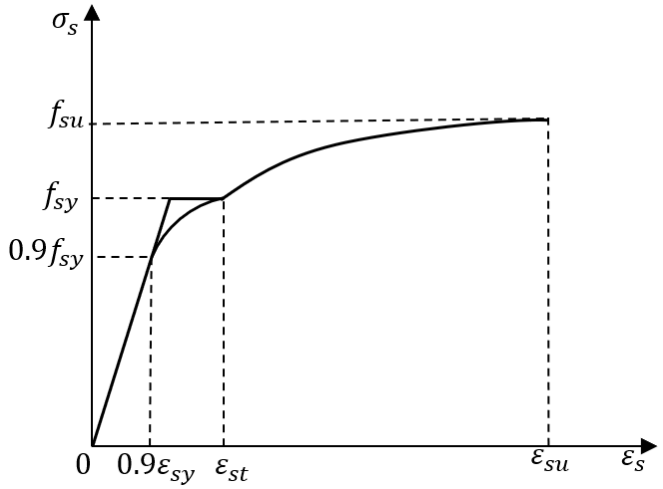


**Fig. 16.** Typical stress-strain curve for structural steels.

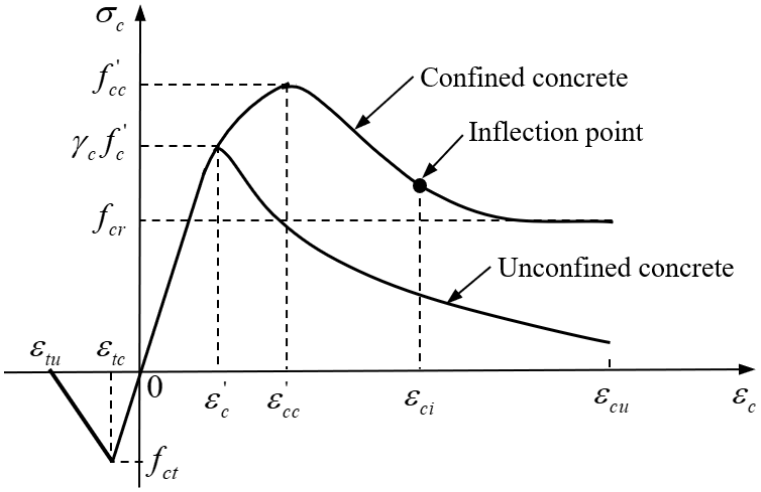


**Fig. 17.** Typical stress-strain curves for confined and unconfined concrete.

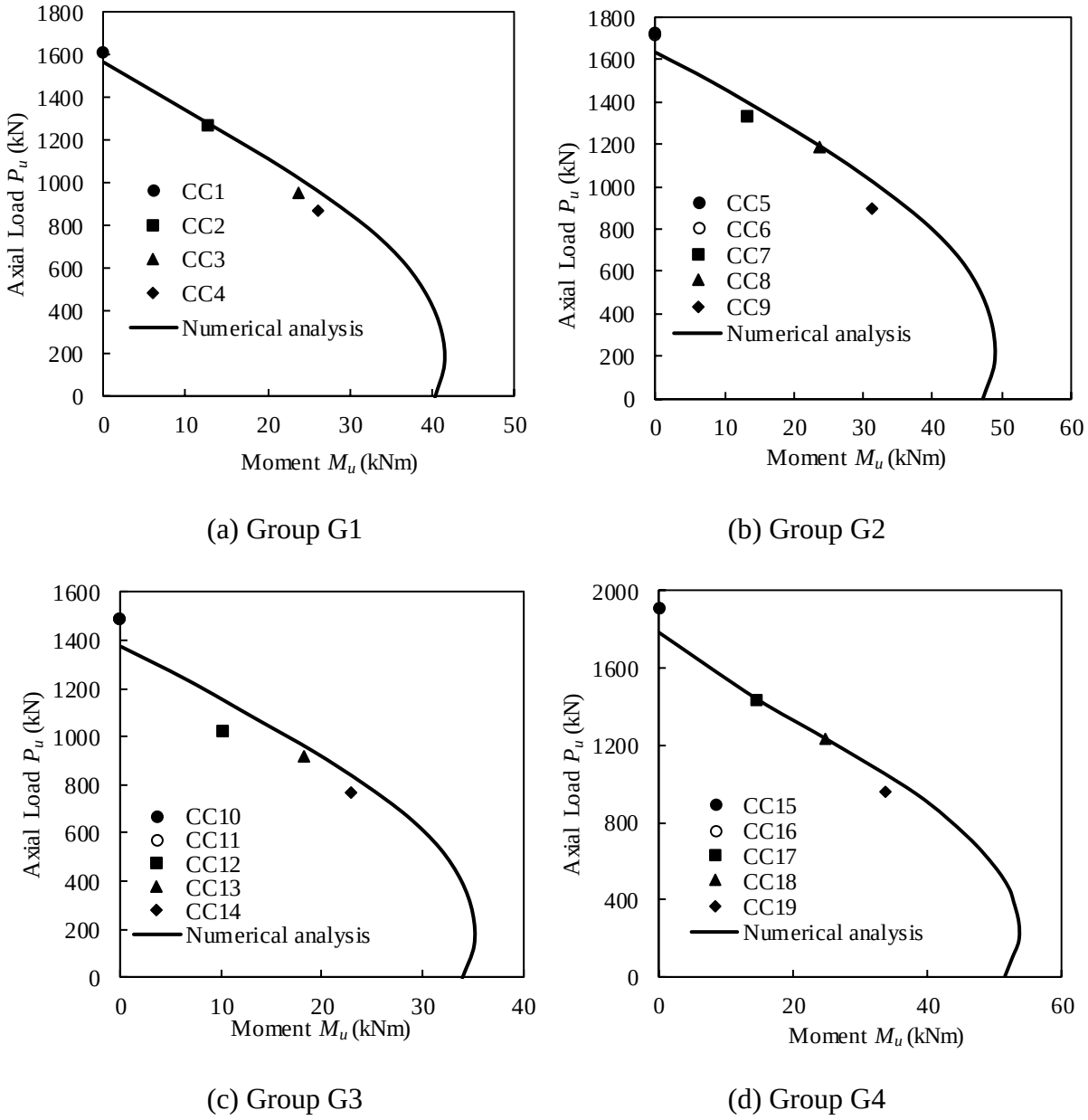


(a) Group G1

(b) Group G2

(c) Group G3

(d) Group G4

**Fig. 18.** Comparison of predicted strength envelopes of circular CFDST columns with test results.

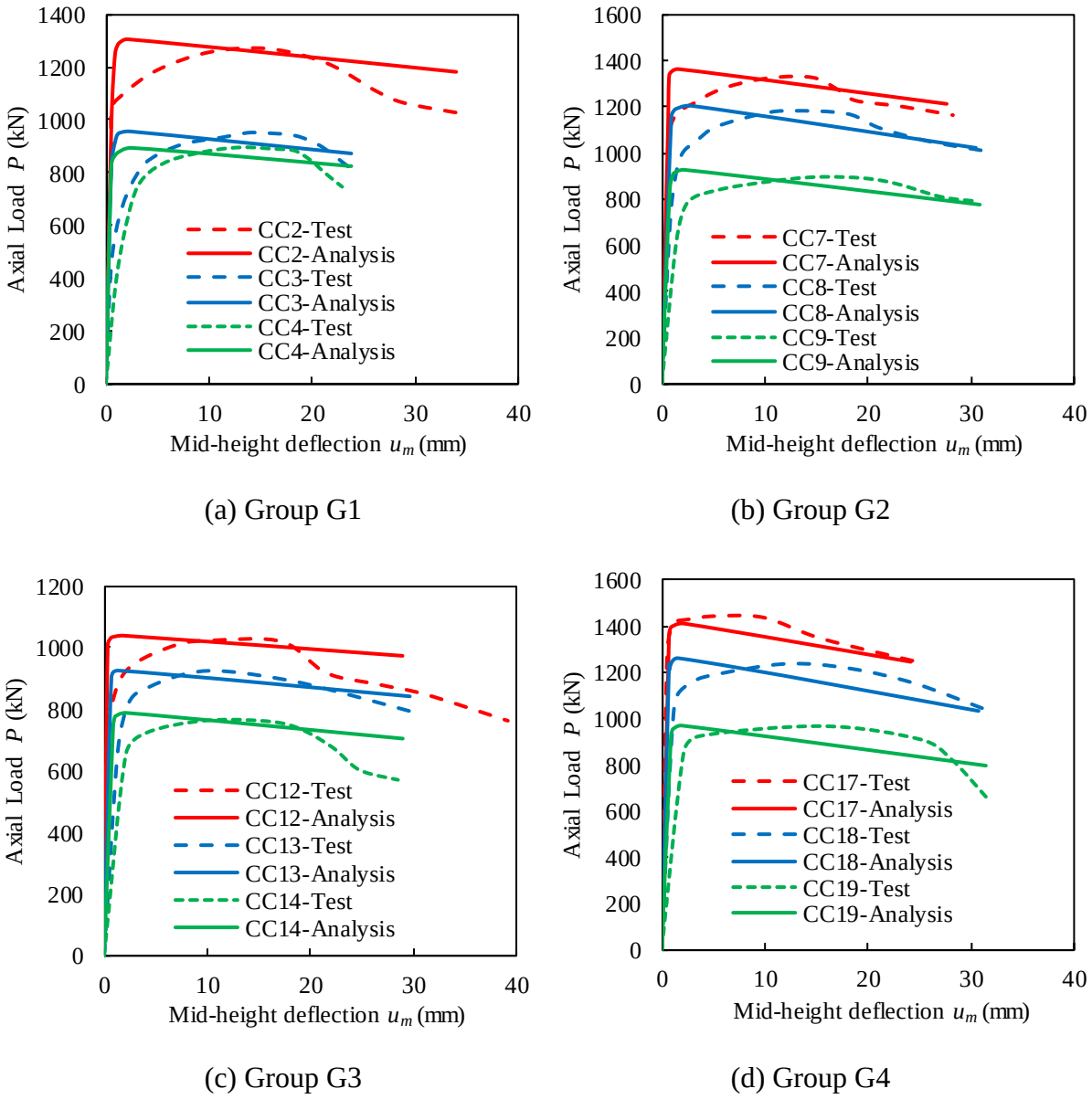


(a) Group G1 (b) Group G2

(c) Group G3 (d) Group G4

**Fig. 19.** Comparison of tested and predicted axial load-mid-height deflection curves of circular CFDST columns.

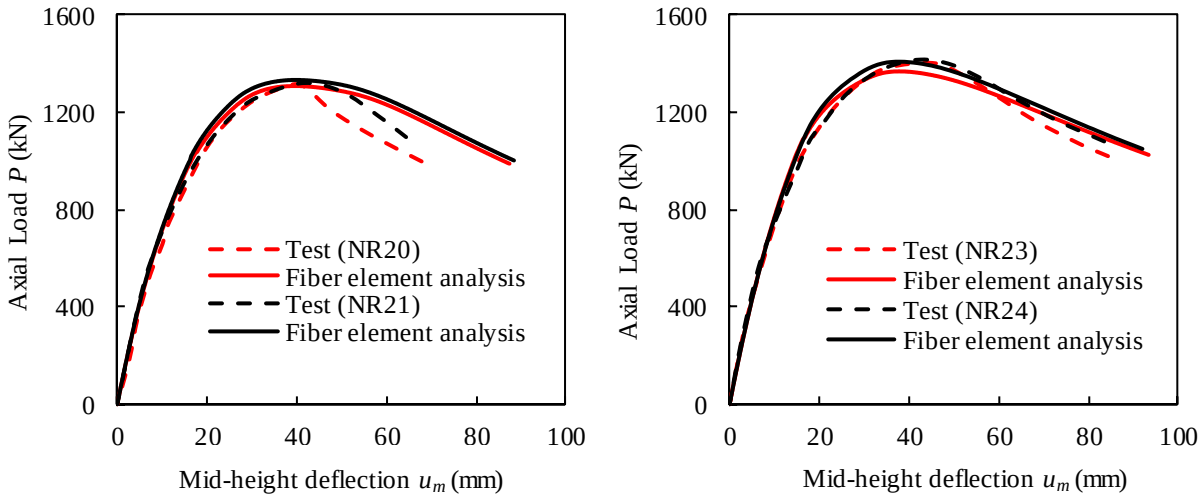


**Fig. 20.** Comparison of predicted and experimental load-mid-height deflection curves of circular CFDST slender columns tested by Ibañez et al. [11].

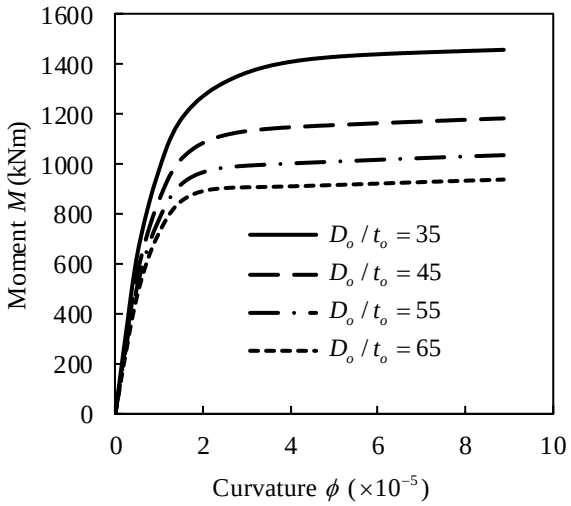


**Fig. 21.** Moment-curvature curves of circular CFDST columns with various $D_o / t_o$ ratios.

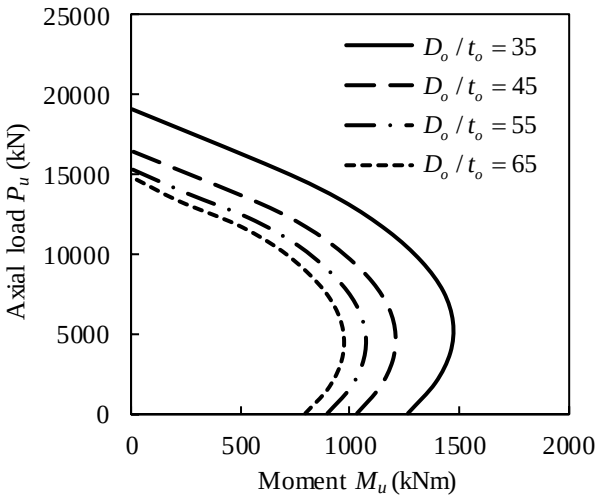


**Fig. 22.** Strength envelopes of circular CFDST columns with various $D_o / t_o$ ratios.

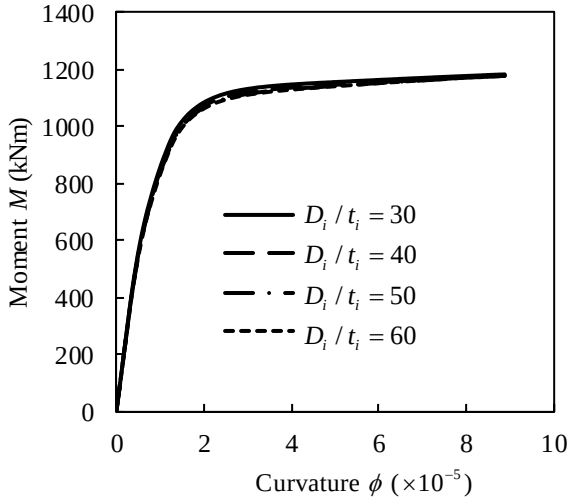


**Fig. 23.** Moment-curvature curves of circular CFDST columns with various $D_i / t_i$ ratios.

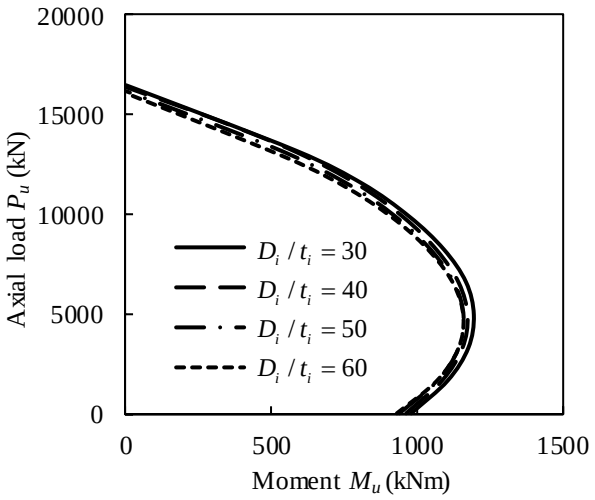


**Fig. 24.** Strength envelopes of circular CFDST columns with various $D_i / t_i$ ratios.

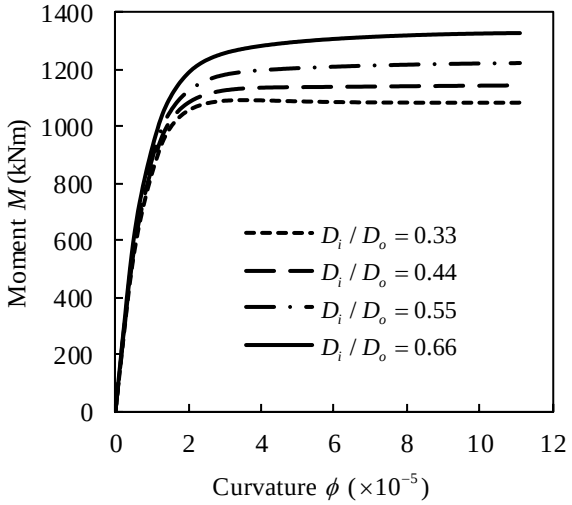


**Fig. 25.** Moment-curvature curves of circular CFDST columns as a function of $D_i / D_o$ ratio.

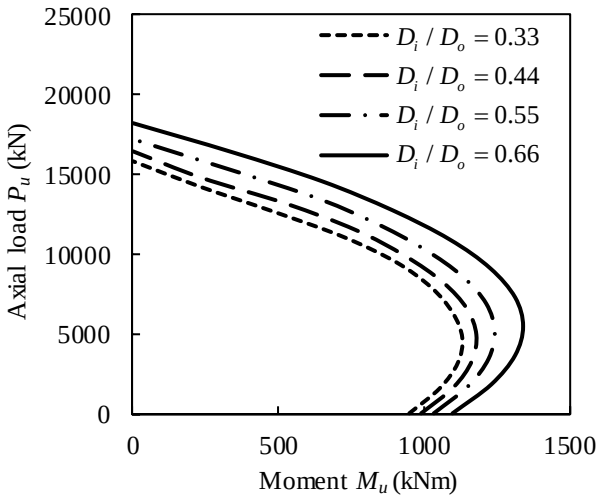


**Fig. 26.** Strength envelopes of circular CFDST columns as a function of $D_i / D_o$ ratio.

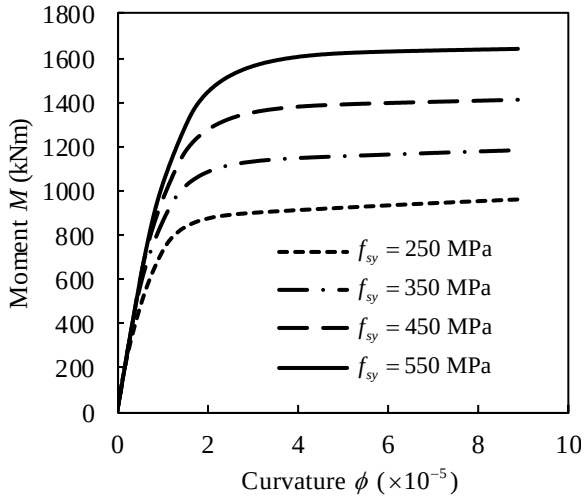


**Fig. 27.** Effects of steel yield strength on the moment-curvature curves of circular CFDST columns.

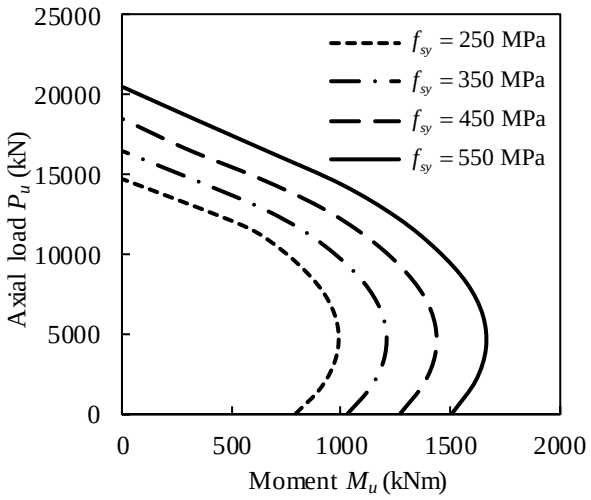


**Fig. 28.** Effects of steel yield strength on the strength envelopes of circular CFDST columns.

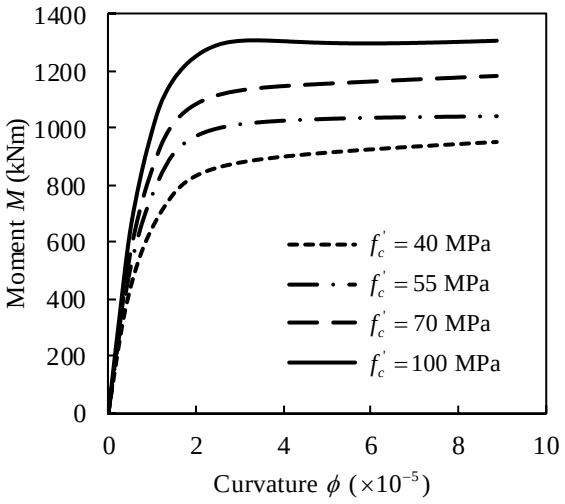


**Fig. 29.** Effects of concrete strength on the moment-curvature curves of circular CFDST columns.

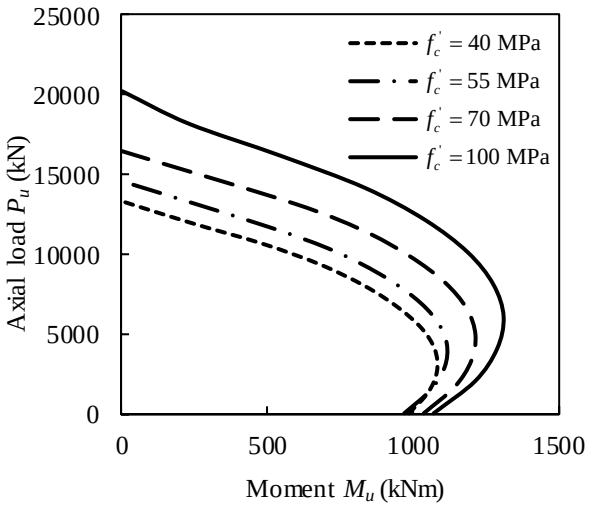


**Fig. 30.** Effects of concrete strength on the strength envelopes of circular CFDST columns.

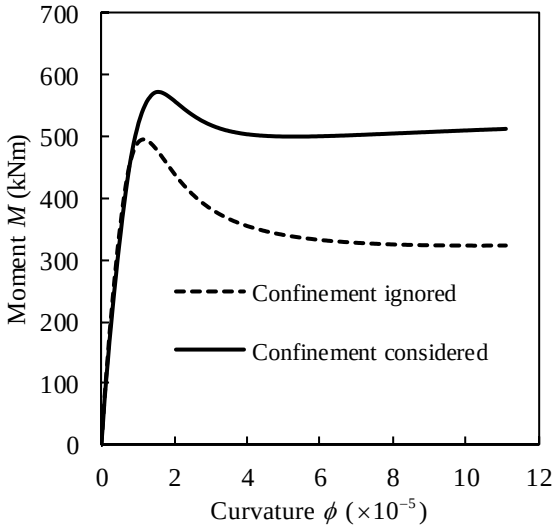


**Fig. 31.** Influences of concrete confinement on the moment-curvature curves of circular CFDST columns.

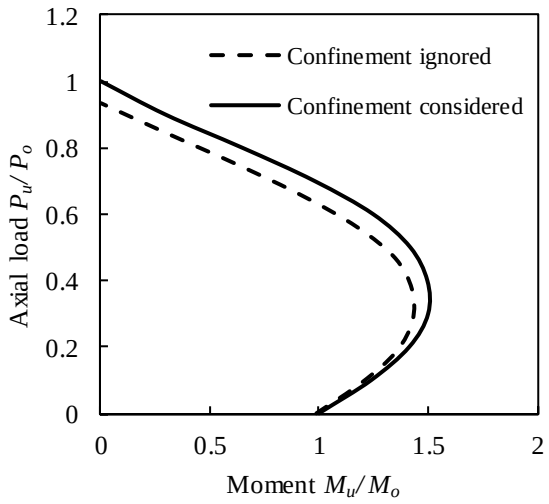


**Fig. 32.** Influences of concrete confinement on the normalized strength envelopes of circular CFDST columns.

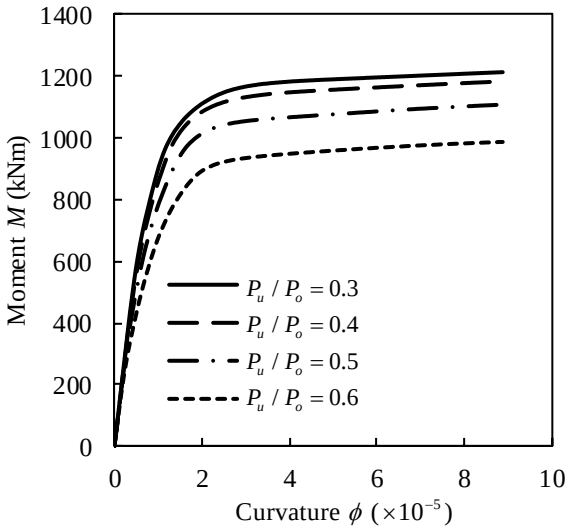


**Fig. 33.** Influences of axial load ratio on the moment-curvature curves of circular CFDST column.

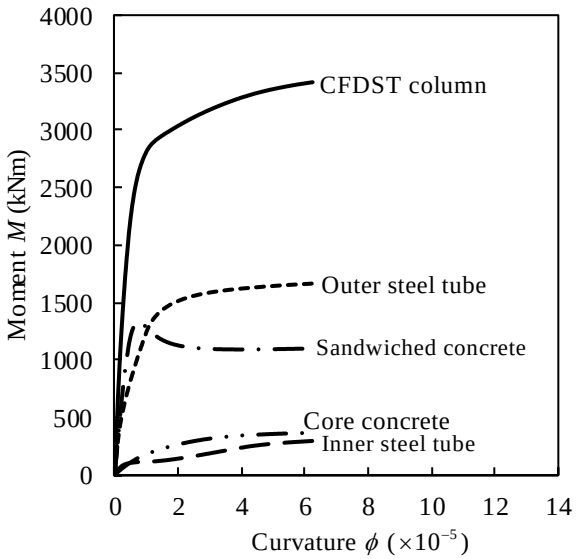


**Fig. 34.** Moment distributions in a circular CFDST beam-column.